Urban Forestry & Urban Greening 54 (2020) 126784

Contents lists available at ScienceDirect

Urban Forestry & Urban Greening

journal homepage: www.elsevier.com/locate/ufug

Spatiotemporal patterns of vegetation phenology along the urban–rural gradient in Coastal Dalian, China

Jun Yang[a,b], Xue Luo[a], Cui Jin[a,*], Xiangming Xiao[c], Jianhong Xia[e]

[a] Human Settlements Research Center, Liaoning Normal University, Dalian, 116029, China
[b] Jangho Architecture College, Northeastern University, Shenyang, 110169, China
[c] Department of Microbiology and Plant Biology, Center for Spatial Analysis, University of Oklahoma, Norman, OK, 73019, USA
[e] School of Earth and Planetary Sciences (EPS), Curtin University, Perth, 65630, Australia

ARTICLE INFO

Handling Editor: Richard Hauer

Keywords:
Urban heat island
Start of growing season
End of growing season
Coastal cities

ABSTRACT

Most studies on vegetation phenology along the urban–rural gradient (URG) have focused on inland cities, with a comparative lack of research on coastal cities despite their different climatic background. We used the normalized difference vegetation index (NDVI), land surface temperature (LST), and land cover data to determine spatiotemporal patterns in vegetation phenology with respect to LST along the URG in China's coastal Dalian sub-province, with a focus on the main city of Dalian and three sub-cities (Pulandian, Wafangdian, and Zhuanghe). Our results were well-correlated with MODIS Land Cover Dynamics Product (MCD12Q2) reference data and matched patterns found in previous studies, indicating that the amplitude method of TIMESAT for obtaining vegetation phenology is practical. Start of growing season (SOS) and end of growing season (EOS) of urban areas were earlier and later than rural areas, respectively. The four urban areas had dissimilar vegetation types and urbanization levels leading to different changes in SOS and EOS along the URG; the average △SOS (the difference in SOS along the URG) and △EOS (the difference in EOS along the URG) of the main and sub-cities were 7.4 and 5.0 d, respectively. Changes in LST along the URG exhibited a non-linear relationship, with the maximum usually appearing 6–8 km from the urban areas. There was a strong linear relationship between vegetation phenology and LST along the URG. The winter–spring and yearly LSTs were negatively correlated with SOS, with both having roughly similar effects. The fall and yearly LSTs had significantly positive correlations with EOS, with the latter having a stronger effect. This study will be helpful for understanding climatic changes arising from urbanization in coastal areas and improving the management and productivity of the ecological environment.

1. Introduction

Vegetation plays an important role in controlling energy flow and other processes in terrestrial ecosystems (Richardson et al., 2013). Vegetation phenology directly reflects the growth cycle of plants and its effects on ecosystem productivity, climate, the carbon balance, and human health. Phenology is affected by precipitation, insolation, latitude and longitude, topography, temperature, and other factors, of which temperature is the most directly important factor while also serving as an indicator of climate change (Cui, 2013; Forkel et al., 2015; Geerken, 2009; Gill et al., 2015; Jeganathan et al., 2014; Jochner et al., 2012). Increasing urbanization in recent decades has resulted in rising urban heat island (UHI) effects and related ecological issues (He et al., 2019; Hu et al., 2019; Liu et al., 2020; Wang et al., 2019a,b,c,d; Xie et al., 2020). As vegetation helps to mitigate the UHI effect, it is important to study differences in vegetation phenology along the urban–rural gradient (URG) to determine ways to mitigate the effects of climate change and ecological problems related to urbanization (Bounoua et al., 2015; Mariani et al., 2016; Weng et al., 2004; Yang et al., 2017; Zhong et al., 2019).

Determining vegetation phenology can involve ground observations, remote sensing data, and modeling. The first method is based on fixed-point observations of individual plants belonging to one or more species, but cannot provide accurate large-scale data due to inherently uneven sampling distribution and excessive time and labor costs (Gazal et al., 2008; Luo et al., 2007; Schaber and Badeck, 2005; Zheng et al., 2013). The development of remote sensing has allowed the collection of data with better spatiotemporal coverage and continuity. Depending on

* Corresponding author.
E-mail addresses: yangjun@lnnu.edu.cn (J. Yang), chenciyixiao@outlook.com (X. Luo), cuijin@lnnu.edu.cn (C. Jin), xiangming.xiao@ou.edu (X. Xiao), c.xia@curtin.edu.au (J. Xia).

https://doi.org/10.1016/j.ufug.2020.126784
Received 14 January 2020; Received in revised form 5 July 2020; Accepted 6 July 2020
Available online 12 July 2020
1618-8667/

the study area, vegetation type, and other factors, data with different temporal or spatial resolutions can be used for monitoring variations in vegetation indexes such as normalized difference vegetation index (NDVI), enhanced vegetation index (EVI), and leaf area index (LAI) that reflect changes in phenology (Chen et al., 2019; Garrity et al., 2011; Hanes and Schwartz, 2011; Verger et al., 2016; Zhang et al., 2004). The modeling approach uses temperature, precipitation, insolation, and latitude and longitude as driving factors to forecast vegetation phenology based on empirical relationships (Chen et al., 2016; Liu et al., 2017; Senf et al., 2017; Villa et al., 2018). Such methods reflect only the "greenness" of vegetation and cannot truly reflect periodic changes in photosynthesis (Jeong et al., 2017; van der Tol et al., 2016; Walther et al., 2016; Wang et al., 2019a,b,c,d). To overcome this issue, researchers have used high-spatial-resolution solar-induced chlorophyll fluorescence (SIF) data to assess the photosynthetic phenology and physiological processes involved more directly and accurately.

Many studies have used remote sensing data to explore the relationship between vegetation phenology, climate change, and urbanization by quantitatively describing differences in vegetation phenology along the URG (Chen and Xu, 2012; Fu et al., 2018; Ren et al., 2018; Wang et al., 2019a,b,c,d; Yao et al., 2017; Zhang et al., 2018). Such studies have shown that urban areas have an earlier start of growing season (SOS) but a later end of growing season (EOS) compared with rural areas and these have generally been attributed to the influence of the UHI effect on vegetation phenology along the URG. Furthermore, vegetation phenology has a significant correlation with land surface temperature (LST). For example, Zhou et al. (2016) used data from 32 major Chinese cities to show that SOS came 9–11 d earlier and EOS 6–10 d later when LST increased by 1 °C. Urban scale also affects vegetation phenology; Li et al. (2016) reviewed 4500 urban areas of various sizes in the United States and showed that SOS came 1.3 d earlier and EOS 2.4 d later when the urban area expanded by a factor of 10.

Previous research on vegetation phenology along the URG has focused on inland cities, but it is not clear whether the different climatic conditions (smaller temperature differences between day and night, and abundant precipitation) of coastal cities could produce different phenological patterns, such as the research of Yao et al. (2017). For example, the sub-province of Dalian in China has undergone rapid urbanization in the past two decades, increasing building surface area and complex morphology (Guo et al., 2020; Yang et al., 2019), and its location on a peninsula within the Bohai Sea makes it a useful representative case study for examining the spatiotemporal responses of vegetation phenology along the URG in coastal cities. We used MODIS NDVI time series data to obtain vegetation phenology, and then used a land cover dynamics product (MCD12Q2) to verify the accuracy of the obtained vegetation phenology. Finally, we used vegetation phenology and MODIS LST data to determine the spatiotemporal patterns of vegetation phenology and LST in Dalian and along the URG and assess the response of vegetation phenology to LST in this region. The results increase our understanding of coastal urban ecosystems and the role of temperature in regulating the vegetation growth cycle.

2. Data and methods

2.1. Study area

The sub-province of Dalian is located in China's Liaoning Province, at the southern end of the Liaodong Peninsula that partially defines the Bohai Sea (120°58′–123°31′ E, 38°43′–40°12′ N) (Fig. 1). The region has a total land area of 1.26×10^5 km^2 (excluding islands), including the main city (also called Dalian (city)) and three sub-cities (Pulandian, Wafangdian, and Zhuanghe). It has a warm temperate continental monsoon climate with maritime characteristics; annual average temperature and precipitation are 10.5 °C and 550–950 mm, respectively, with a dominant vegetation type represented by warm temperate deciduous broad-leaved forests.

2.2. Data sources and processing

Over the past 20 years, Dalian has experienced rapid urbanization and the development of complex human activity. The data sources included: China's Land Use/Cover Datasets (CLUDs; data with a high spatiotemporal resolution), MOD13Q1 (Collection 6) (NASA LP DAAC, 2015a), MOD11A2 (Collection 6) (NASA LP DAAC, 2015b), and MCD12Q2 (Collection 6) (NASA LP DAAC, 2019) as shown in Table 1.

The intersections of contiguous developed land in the CLUDs were used to define the urban area for the four cities studied. The center of each city was then used to establish 10 concentric buffer zones of 1 km each that defined the URG for each urban area (the outer buffer is shown in Fig. 1). The LST data were extracted from the QA layer of the MOD11A2 product, using data with mandatory QA flags of 00. These data were combined with known physiological demands (such as temperature accumulation) of vegetation growth with reference to LST to supplement deficiencies in existing research, which has not comprehensibly defined the impacts of LST on vegetation phenology during the day, night, and different time periods (Deng et al., 2019; Wang et al., 2019a,b,c,d; Yuan et al., 2018). Next, the diurnal and nocturnal LSTs (LST_D and LST_N, respectively) were calculated along with the mean LST (LST_{Mean}, average of LST_D and LST_N). Our analysis covered the winter-spring (LST_{WS}, from December of the previous year to May of the following year) and fall (LST_F, from September to November) of each year studied and the full year (LST_Y) periods; the subscripts here were also used to distinguish time periods for different data, e.g., LST_{F_N} for nocturnal fall and LST or LST_{Y_MEAN} for annual mean. To verify the feasibility of the proposed method, we extracted the effective greenup and dormancy layers from the QA_Overall layer of MCD12Q2 data based on QA Overall Class values ≤ 1, as per the previous definitions of SOS and EOS (Sakamoto, 2018), which were designated as $SOS_{MCD12Q2}$ and $EOS_{MCD12Q2}$, respectively.

2.3. Research method

2.3.1. Obtaining phenology using the amplitude method

The Savitzky–Golay (S–G) filtering method can describe complex and small changes in NDVI time-series data while suppressing noise from clouds and atmospheric change (Cao et al., 2018; Chen et al., 2004; Jönsson and Eklundh, 2004; Tan et al., 2011). We used TIMESAT software to apply this method for a smooth reconstruction of the MODIS NDVI time-series data based on the amplitude method, which uses the difference between annual maximum and minimum NDVI to determine SOS and EOS based on the date when the fitted curve rises or falls to a certain amplitude ratio. We used a 30 % amplitude as this has been shown to best match ground observations; an adaptive intensity of 2.0 and an S–G window size of 2 were used to extract vegetation phenology (Yu et al., 2014; Zhao et al., 2016). Given that human activity can create outliers in vegetation phenology, the effective ranges of SOS and EOS were set to 50–180 and 240–330 d, respectively, to ensure data accuracy (Cong et al., 2012; White et al., 2009; Zhang et al., 2006).

2.3.2. Calculating differences in vegetation phenology and LST along the URG

After comprehensively considering differences in climatic environment, urbanization level, and data quality (Zhou et al., 2016), we separately calculated the average SOS and EOS of the four urban areas and their rural buffer zones from 2001 to 2017, then compared differences in vegetation phenology along the URG using the following equations:

$$\Delta SOS_i = SOS_{ub} - SOS_{ri} \tag{1}$$

$$\Delta EOS_i = EOS_{ub} - EOS_{ri} \tag{2}$$

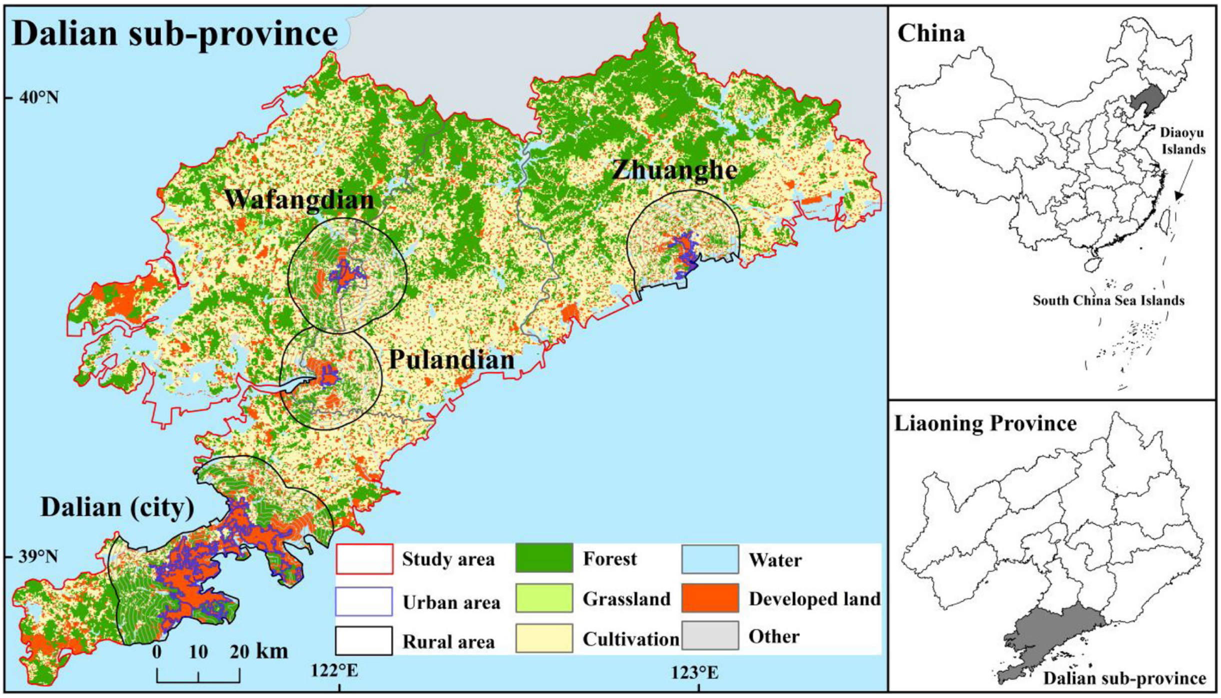

Fig. 1. Location of the sub-province of Dalian and 2015 land-use classification; urban area and rural area used for analysis are marked for the main city and three sub-cities.

Table 1
Description and sources of data.

Data product	Attributes	Source	Layers	Temporal coverage
MOD13Q1	250 m/16 d	https://lpdaac.usgs.gov/	250 m 16 days NDVI,250 m 16 days VI Quality detailed QA	2001 – 2017
MOD11A2	1000 m/8 d	https://lpdaac.usgs.gov/	LST_Day_1 km,QC_Day, LST_Night_1 km,QC_Night	2001 – 2017
MCD12Q2	500 m/yr	https://lpdaac.usgs.gov/	Greenup, Dormancy, QA_Overall	2001 – 2016
China's Land Use/Cover Datasets (CLUDs)	100 m	http://www.resdc.cn/		2000,2005, 2010,2015

where SOS_{ub}, EOS_{ub} and SOS_{ri}, EOS_{ri} represent the average SOS and EOS of the urban and i^{th} buffer zone, respectively, and ΔSOS_i, ΔEOS_i represent the difference in SOS and EOS along the URG. When ΔSOS_i and ΔEOS_i are negative, the urban SOS and EOS occur earlier than rural ones, and vice versa.

Differences in LST along the URG were calculated in the same manner:

$$\Delta LST_i = LST_{ub} - LST_{ri} \tag{3}$$

where LST_{ub} and LST_{ri} represent the average LST of the urban and rural areas' i^{th} buffer zone, respectively, and ΔLST_i represents the difference in LST along the URG. When ΔLST_i is negative, the urban LST is lower than the rural, and vice versa.

3. Results

3.1. Verification of the vegetation phenology results

We verified our vegetation phenology results by comparison with other research and MCD12Q2 data. As shown in Table 2, we found that the spatial characteristics of vegetation phenology were consistent with previous research (Fu et al., 2018; Hou et al., 2014; Li et al., 2014; Yao et al., 2017; Yu et al., 2017, 2014; Zhao et al., 2016), but our inter-annual variations differed to a certain extent from comparable work (Ren et al., 2018; Zhao et al., 2015). The difference was likely due to general differences in study area/period, data sources, climatic setting, urban scale, and vegetation type as well as specific factors affecting the influence of Dalian's urbanization on local vegetation phenology during the study period (Krehbiel et al., 2016; Liang et al., 2016; Stewart and Oke, 2012; Zipper et al., 2016).

The SOS and EOS obtained from MOD13Q1 were verified against $SOS_{MCD12Q2}$ and $EOS_{MCD12Q2}$, respectively (Fig. 2a and b). SOS differences ranged from −23 to 35 d (with an average difference of 6.7 d). Of the total SOS pixels, 15 % were earlier relative to $SOS_{MCD12Q2}$, while 85 % were delayed. EOS differences ranged from −32 to 31 d (average difference −0.6 d) with the largest difference occurring in the northern woodlands. Of the total EOS pixels, 51 % were earlier relative to $EOS_{MCD12Q2}$ and 49 % were delayed. As for temporal patterns (Figs. 2c, d), the correlation between $SOS_{MCD12Q2}$ and SOS was significant ($r = 0.74$, $p < 0.01$), although the root mean square error (RMSE) of SOS was smaller than that of $SOS_{MCD12Q2}$. Compared with our SOS,

Table 2
Vegetation phenology compared with other studies.

	This Study	Fu et al. (2018)	Hou et al. (2014)	Li et al. (2014)	Yao et al. (2017)	Yu et al. (2017)	Yu et al. (2014)	Zhao et al. (2016)
SOS (Day of year)	110 – 170		110 – 170	131 – 140	112 – 161	100 – 140	100 – 140	110 – 160
EOS (Day of year)	280 – 330	285 – 325	240 – 300	255 – 264	273 – 300	280 – 320	265 – 300	295 – 345

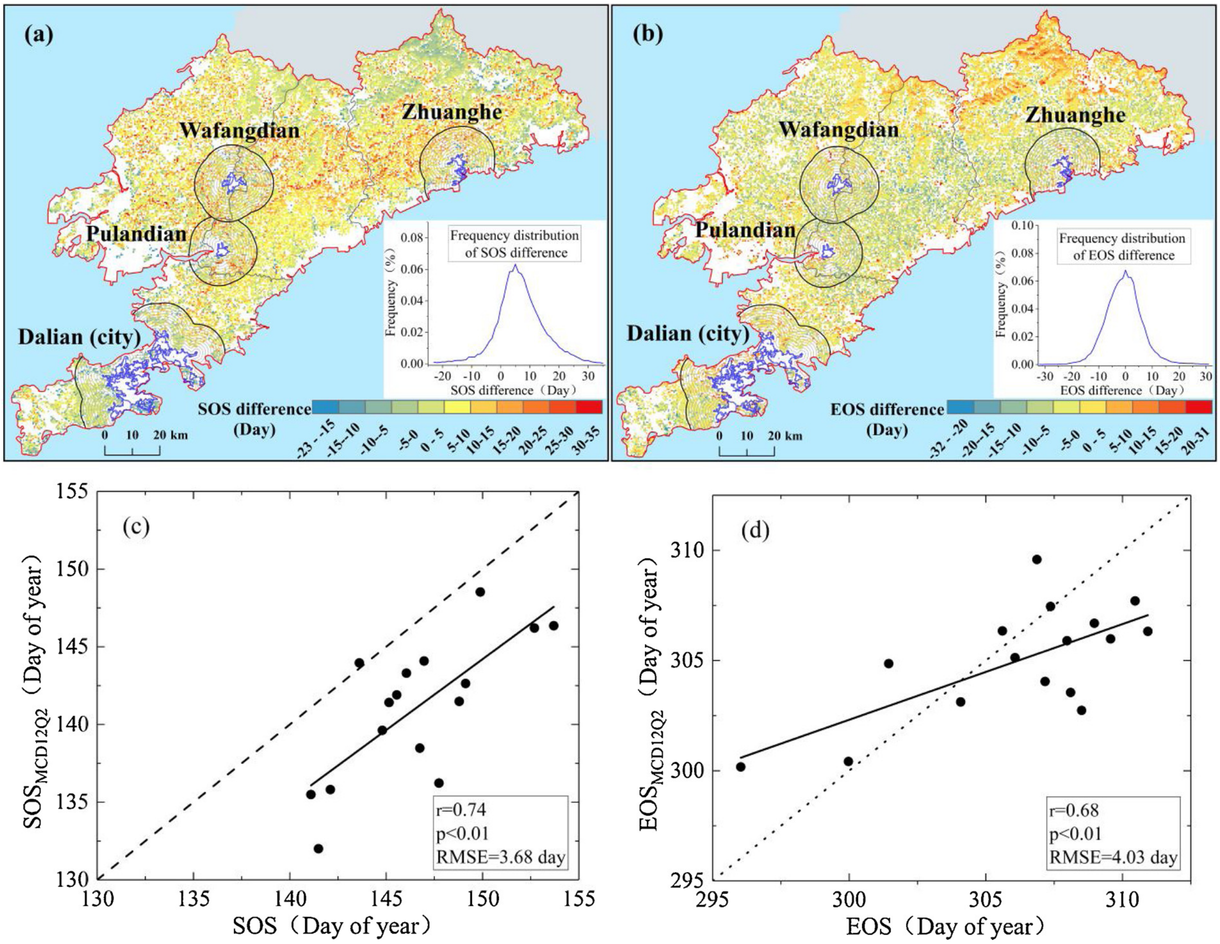

Fig. 2. Spatial comparison of (a) SOS and $SOS_{MCD12Q2}$ and (b) EOS and $EOS_{MCD12Q2}$ and temporal relationship between (c) SOS and $SOS_{MCD12Q2}$ and (d) EOS and $EOS_{MCD12Q2}$.

$SOS_{MCD12Q2}$ showed an overall earlier trend that generally shifted its peak forward, consistent with previous studies (Vintrou et al., 2014; Wang et al., 2017; Xin et al., 2015). Similarly, there was a good correlation between $EOS_{MCD12Q2}$ and EOS ($r = 0.68$, $p < 0.01$), with an RMSE for the latter of 4.03 d.

The differences between vegetation phenology in this study and MCD12Q2 can be explained by the fact that $SOS_{MCD12Q2}$ and $EOS_{MCD12Q2}$ were calculated based on EVI whereas we used NDVI. In addition, the amplitude ratio for $SOS_{MCD12Q2}$ and $EOS_{MCD12Q2}$ was 15 % as compared to 30 % in this study. Overall, the comparison with prior research and MCD12Q2 data verified the accuracy of our results, indicating that the proposed method for obtaining vegetation phenology was feasible and could serve as a reference for the study of vegetation phenology in other coastal cities.

3.2. Spatiotemporal patterns of vegetation phenology along the URG

The average SOS for the entire Dalian sub-province from 2001 to 2017 ranged from 110 to 170 d with an overall average of 145.8 d, while the average EOS ranged from 280 to 330 d with an overall average of 307.7 d (Fig. 3). Dalian (city) had the earliest average SOS (137.8 d), followed by Zhuanghe (143.9 d), Wafangdian (146.2 d), and Pulandian (153.3 d). Similarly, Dalian (city) also had the latest EOS (313.2 d), preceded by Wafangdian (308.7 d), Zhuanghe (307.8 d), and Pulandian (302.8 d). The SOSs in the coastal areas of Pulandian, Zhuanghe, and Wafangdian were 9.2 d later than in the northern woodlands. The EOSs in Dalian (city) and the northern woodlands were the latest, 1.9 d after the EOSs in the coastal areas of Pulandian, Zhuanghe, and Wafangdian. Over time, the overall SOS clearly came earlier by 0.56 d/yr ($r^2 = 0.48$, $p < 0.01$), though this varied significantly from year to year; the overall EOS arrived later by 0.57 d/yr ($r^2 = 0.41$, $p < 0.01$) with similar year to year fluctuations.

Within the urban buffer zones, SOS grew gradually later with increasing distance from three of the four urban centers (Fig. 4), with a delay of 5.4 d for Dalian (city) ($r^2 = 0.93$, $p < 0.01$), 11.1 d for Pulandian ($r^2 = 0.82$, $p < 0.01$), and 13.1 d for Zhuanghe ($r^2 = 0.86$, $p < 0.01$); the effect was particularly pronounced within 2–4 km. However, Wafangdian showed a very different trend, with an average delay of 0.7 d for 1–7 km followed by an abrupt earlier trend to 1.5 d for 8–10 km. EOS grew gradually earlier with distance from urban areas—11.4 d for Pulandian ($r^2 = 0.71$, $p < 0.01$) and 7.9 d for Zhuanghe ($r^2 = 0.94$, $p < 0.01$). For Dalian (city), there was a gradual delay in EOS for 1–6 km, followed by an abrupt earlier trend for 7–10 km. For Wafangdian, EOS grew earlier with distance—1.7 d for 1–7 km to 0.2 d for 8–10 km.

3.3. Spatiotemporal patterns in LST along the URG

The spatial patterns of LST_{Y_D}, LST_{Y_N}, and LST_{Y_Mean} were all similar in being higher closer to urban areas (Fig. 5). From 2001–2017, annual overall LST_{Y_D} ranged from 13 to 17 °C (average 14.7 °C), LST_{Y_N} ranged from 2 to 5 °C (average 2.5 °C), and LST_{Y_Mean} ranged from 7 to 11 °C (average 8.4 °C). In all cases, the temperatures in Dalian (city) were the highest and those in the northern mountainous areas were the lowest. All cases experienced annual increases at an overall rate of 0.03 °C/year.

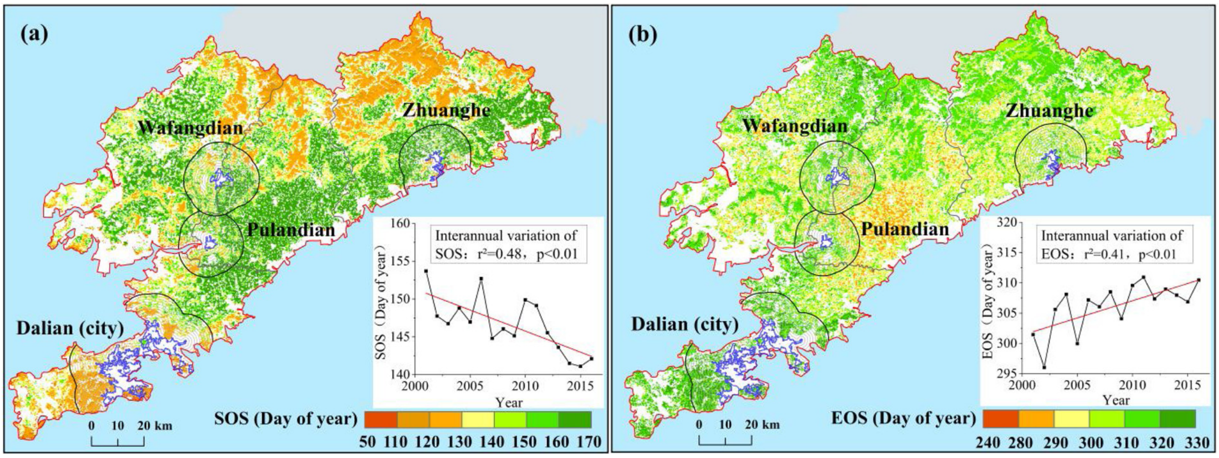

Fig. 3. Temporal and spatial patterns of average (a) SOS and (b) EOS in Dalian sub-province from 2001–2017.

The △LST along the URG showed a significant non-linear relationship (Fig. 6). There was an initial trend of gradual decline in LST with increasing distance from the urban center, with △LST reaching its maximum at 6–8 km, after which it gradually decreased with further distance. The $\triangle LST_{WS\_D}$, $\triangle LST_{WS\_N}$, and $\triangle LST_{WS\_Mean}$ were 2.1, 3.0, and 2.6 °C, respectively, peaking at 6, 7–8, and 7 km, respectively. The $\triangle LST_{F\_D}$, $\triangle LST_{F\_N}$, and $\triangle LST_{F\_Mean}$ were 2.5, 4.2, and 3.2 °C, respectively, peaking at 8, 6, and 8 km, respectively. The $\triangle LST_{Y\_D}$, $\triangle LST_{Y\_N}$, and $\triangle LST_{Y\_Mean}$ were 2.3 °C, 2.7 °C, and 2.6 °C, respectively, peaking at 7 km for the first two; LST_{Y_Mean} peaked at 7 km for the city of Dalian but at 6 km for Pulandian, Wafangdian, and Zhuanghe.

3.4. Relationship between vegetation phenology and LST along the URG

SOS had a significantly negative correlation with LST_{WS} and LST_Y; the correlation between SOS and LST_{Y_D} was highest at Zhuanghe (r = -0.95, $p < 0.01$) (Table 3). EOS was positively correlated with LST_F and LST_Y; the correlation between EOS and LST_{Y_D} was highest at Pulandian ($r = 0.96$, $p < 0.01$).

As shown in Fig. 7, when LST_{WS_D}, LST_{WS_N}, and LST_{WS_Mean} increased by 1 °C, SOS occurred 3.6, 2.5, and 2.8 d earlier, respectively (average 3.0 d). LST_{Y_D}, LST_{Y_N}, and LST_{Y_Mean} had negative correlations with SOS; an increase of 1 °C in LST caused SOS to occur 3.2, 2.7, and 2.9 d earlier (average 2.9 d). LST_{WS} and LST_Y had similar effects with regard to earlier SOS. When LST_{F_D}, LST_{F_N}, and LST_{F_Mean} increased by 1 °C, EOS was delayed by 2.0, 1.2, and 1.6 d, respectively (average 1.6 d). EOS was positively correlated with LST_{Y_D}, LST_{Y_N}, and LST_{Y_Mean}: when LST increased by 1 °C, these were delayed by 2.2, 1.9, and 2.0 d, respectively (average 2.0 d). The delay effect of LST_Y on EOS was significantly greater than that of LST_F.

4. Discussion

4.1. Impact of LST on vegetation phenology

This study's focus on differences in LST along the URG in the winter–spring, fall, and annual periods in terms of day, night, and mean values was intended to address the existing lack of understanding regarding the comprehensive impact of LST on vegetation phenology. LST was consistently and significantly higher with increasing proximity to urban areas, following a clear non-linear relationship; this was consistent with Han and Xu (2013). Peng et al. (2012) assessed 419 global cities and showed that the average annual surface UHI intensity was higher during daytime than nighttime (1.5 ± 1.2 °C and 1.1 ± 0.5 °C, respectively), which contradicts our finding that $\triangle LST_{Y\_D}$ (2.3 °C) was lower than $\triangle LST_{Y\_N}$ (2.7 °C). This conflict may relate to differences in the respective delineations of urban versus rural areas, urban scale, and climatic backgrounds between the two studies (Busetto et al., 2010; Fu and Weng, 2018; Liu et al., 2016; Wu et al., 2016; Yu et al., 2010). Our SOS showed a significantly negative correlation with $\triangle LST_{WS}$ and $\triangle LST_Y$, whereas EOS showed a strong positive correlation with $\triangle LST_F$ and $\triangle LST_Y$; these results are consistent with previous research.

The LSTs exhibited a non-linear relationship along the URG, with the maximum △LST difference appearing at 6–8 km from urban areas in most cases. This had a direct impact on the vegetation phenology. Unlike the other urban areas, the SOS and EOS for Wafangdian did not show any clear trend along the URG. Fitting by segments along the URG from Wafangdian identified the segmentation of the fitting line for

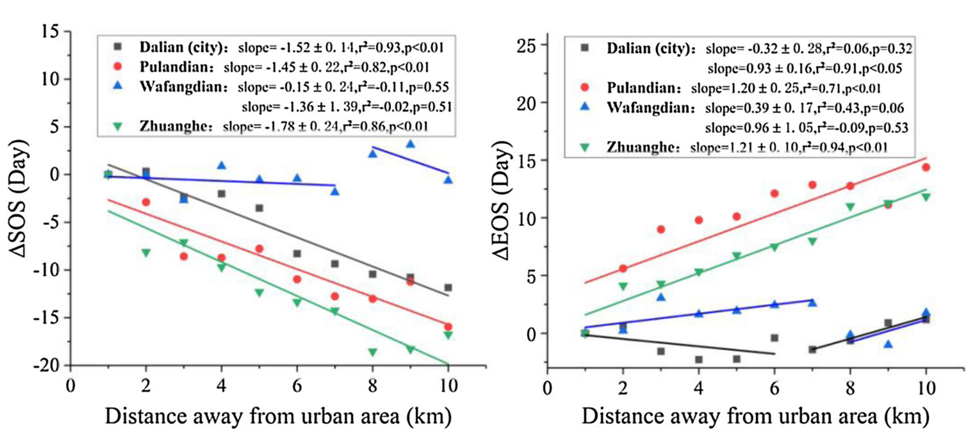

Fig. 4. Change in SOS and EOS within the URGs of the four studied cities.

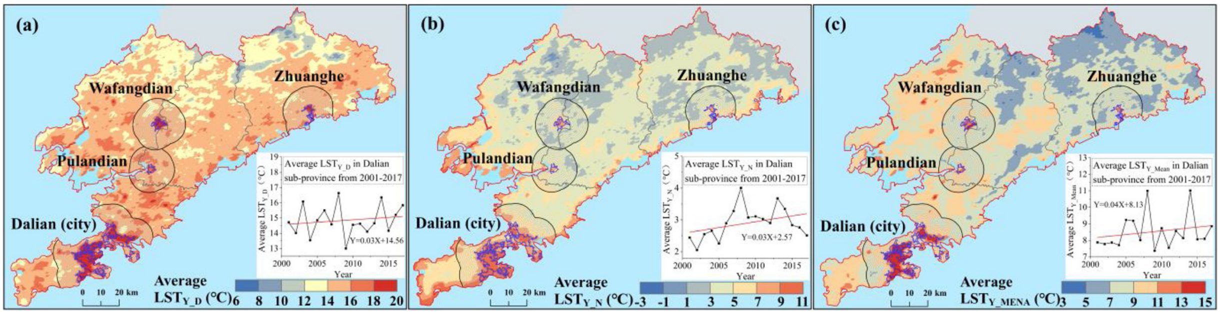

Fig. 5. Temporal and spatial patterns of land surface temperature (°C) from 2001–2017 for (a) LST_{Y_D}, (b) LST_{Y_N}, and (c) LST_{Y_Mean}.

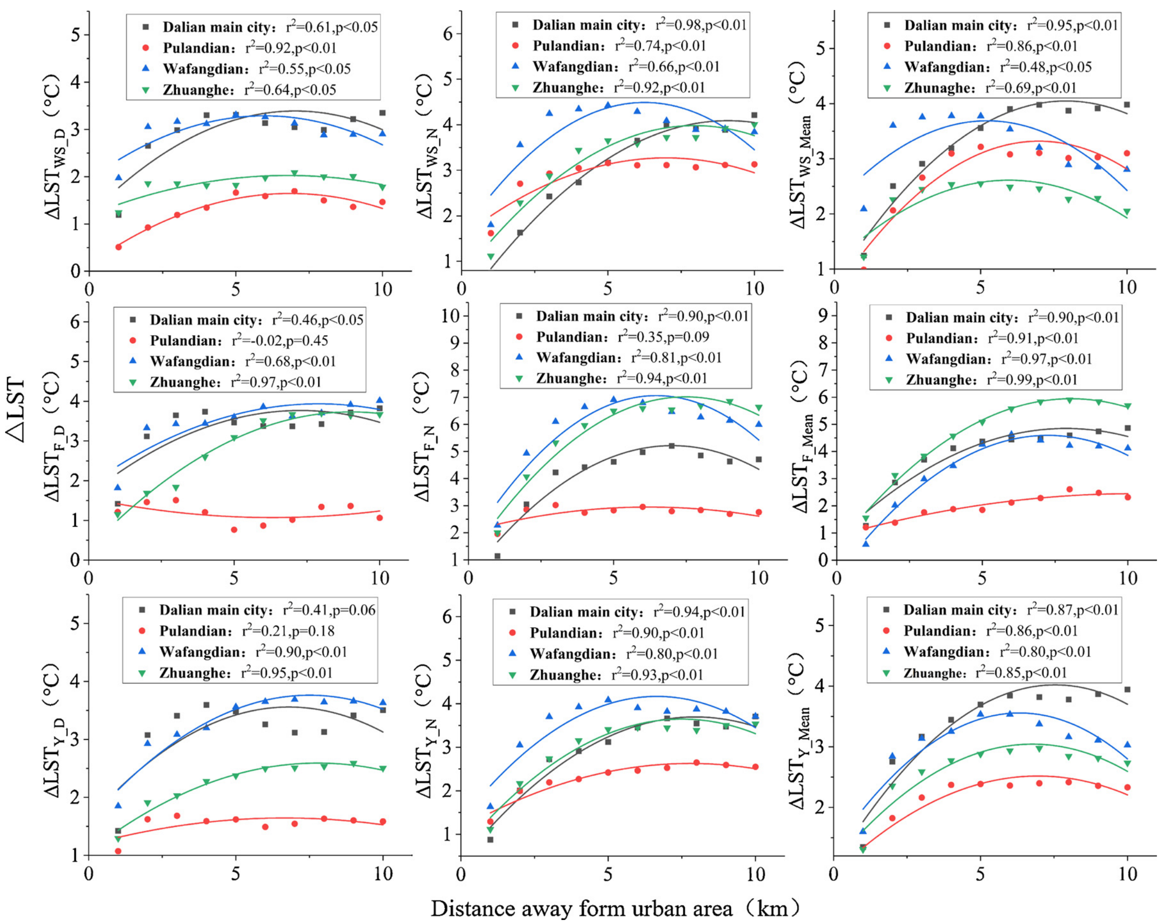

Fig. 6. Differences in land surface temperature along the URG for winter-spring (top row), fall (middle row), and annual (bottom row) with respect to diurnal (left column), nocturnal (middle column) and mean (right column) periods.

△SOS to a point at 7 km while the maximum difference for both $\triangle LST_{WS}$ and $\triangle LST_{Y}$ appeared at 6 km; the segmentation point of the △EOS fitting line appeared at 7 km while the maximum differences for $\triangle LST_{F}$ and $\triangle LST_{Y}$ appeared at 7 and 6 km, respectively. These results matched those of Han and Xu (2013), who determined that urbanization affected vegetation phenology for up to 6 km from urban areas. The lack of clear trends in vegetation phenology for Wafangdian can be explained in several ways. First, its urban/rural delineation results in large amounts of forest contained in the latter, for which SOS and EOS are earlier and later, respectively. Second, its location close to

Table 3
Correlation between vegetation phenology and land surface temperature along the URGCorrelation.

	SOS/LST_{WS}			SOS/LST_{Y}			EOS/LST_{F}			EOS/LST_{Y}		
	Day	Night	Mean	Day	Night	Mean	Day	Night	Mean	Day	Night	Mean
Dalian (City)	−0.53	−0.92	−0.84	−0.40	−0.84	−0.75	−0.15	−0.25	−0.09	−0.22	−0.07	−0.10
Pulandian	−0.83	−0.80	−0.84	−0.62	−0.90	−0.84	−0.31	0.71	0.90	0.74	0.96	0.93
Wafangdian	−0.25	−0.10	−0.36	0.13	0.06	−0.06	0.23	0.45	0.30	0.25	0.38	0.48
Zhuanghe	−0.80	−0.92	−0.54	−0.95	−0.90	−0.83	0.92	0.87	0.92	0.91	0.86	0.75

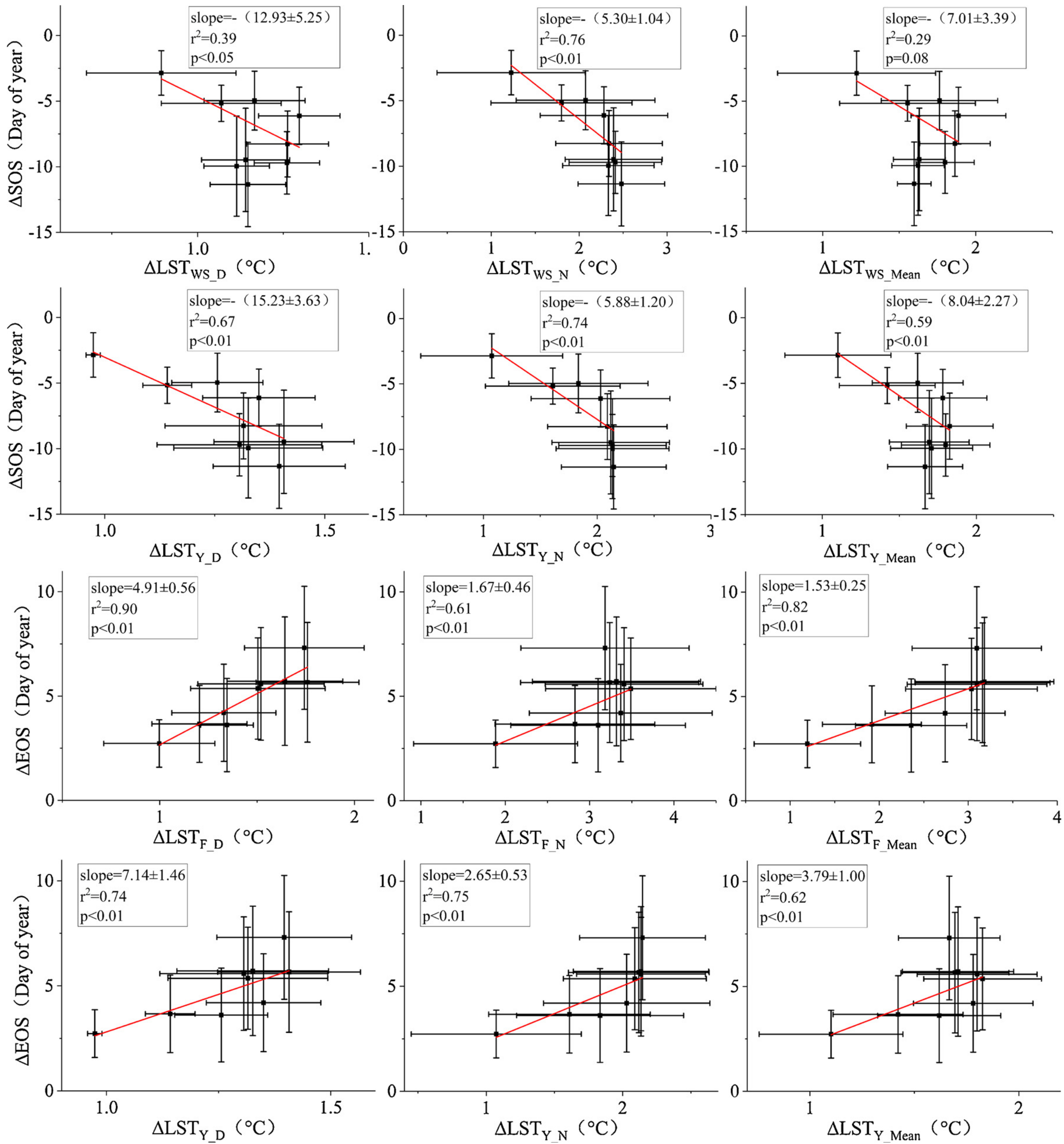

Fig. 7. Relationships between vegetation phenology (SOS or EOS) and land surface temperature for various combinations of conditions along the URG.

Pulandian and the higher LSTs of Pulandian has a stronger influence on the vegetation phenology of Wafangdian.

4.2. Uniqueness of vegetation phenology along the URG in coastal cities

Studies on the differences in vegetation phenology along the URG have had different final results due to differences in selected data, regions, study periods, urbanization levels, and statistical methods (Table 4). For example, the △SOS and △EOS determined for Dalian were smaller than those for Beijing and northeastern China. Comparing the results of 32 major cities in China, the differences in vegetation phenology along the URG in inland cities were evident, and more in line with the fitted curve than coastal cities. Moreover, along the eastern coast of the United States, △SOS by latitude was −15–0 d and △EOS was 0–20 d; △SOS in New York was 7 d, similar to the 7.4 d determined for Dalian. Such comparisons of our results and those of other studies show that differences in vegetation phenology along the URG in coastal cities show a smaller trend than for inland cities, which is closely related to the unique climate background of coastal cities.

Dalian sub-province was selected as the study area to assess the uniqueness of vegetation phenology in coastal cities with a different climatic background than the more commonly studied inland settings. Vegetation phenology in such cities is more sensitive to temperature, meaning that a given increase in LST has a greater impact than for inland cities (Wang et al., 2015, 2017; Workie and Debella, 2018; Zhang et al., 2006). In addition, past research has shown that LST has a stronger impact on SOS than EOS (Wang et al., 2017; Yuan et al., 2018; Zhao et al., 2015), which is consistent with the findings of this study. Second, Dalian is greatly affected by the maritime monsoon, resulting in higher precipitation than inland cities. Vegetation growth is closely related to precipitation amount, with an obvious lag effect on vegetation phenology (Du et al., 2019; Sohoulande Djebou et al., 2015; Workie and Debella, 2018). Consequently, the SOS in coastal cities tends to be later than that in inland cities. Third, a coastal city's climatic environment is jointly determined by its proximity to the ocean, its vegetation structure, and its urbanization level, which then indirectly

Table 4
Differences in vegetation phenology along urban-rural gradients compared with other studies.

	Han et al.(2013)	Li et al. (2016)	Yao et al. (2017)	Luo (2013)	Zhou et al. (2016)	This paper
Data	SPOT/VGT NDVI	MCD12Q2	MOD13A2	MOD13A2	MYD13Q1	MOD13Q1
Temporal coverage	2002 – 2009	2003 – 2012	2001 – 2015	2002 – 2009	2007 – 2013	2001 – 2017
Fitting method	S-G		S-G		Double logistic	S-G
Calculate Difference	$\triangle P = P_r - P_{ub}$	$\triangle P = P_{ub} - P_r$	$\triangle P = P_{ub} - P_r$	$\triangle P = P_{ub} - P_r$	$\triangle P = P_{ub} - P_r$	$\triangle P = P_{ub} - P_r$
Study area	Yangtze River Delta, China	United States	Northeast China	Beijing, China	China's 32 major cities	Dalian, China
△SOS	Shanghai:6 – 16, Nanjing:-8 – 4Changzhou:-2 – 3,Wuxi:-2 – 6Suzhou:-3 – 6,Hangzhou:2 – 6	East Coast of the United States at the same latitude as Dalian:-15 – 0 (New York:7)	− 16.8	− 20	− 11.9	− 7.4
△EOS	Shanghai:-13 – 1, Nanjing:-11 – 1Changzhou:-17 – 0,Wuxi:-10-3 Suzhou:-8-1,Hangzhou:7-1	East Coast of the United States at the same latitude as Dalian:0 – 20	15.96	15	5.4	5.0

affects its vegetation phenology (Balica et al., 2012; Tarawally et al., 2018).

LST increases may cause coastal areas to face more ecological problems (Zikra and Suntoyo, 2015), indirectly affecting vegetation phenology. For example, earlier SOSs and later EOSs prolong the growing season, increasing the gross primary productivity (GPP) and net primary productivity (NPP) of the vegetation. Therefore, studying reasons behind differences in vegetation phenology between inland and coastal cities can improve agricultural management in coastal regions while better quantifying the impact of urbanization on the ecological environments of coastal cities.

4.3. Uncertainties

Although our results provided a strong basis for predicting the impact of urbanization on the ecological environment of a coastal setting like Dalian, there were several limitations to our approach. First, the MOD13Q1 data had a spatial resolution of 250 m, meaning that each pixel represented 6.25×10^4 m^2, such that details of land use or vegetation status could be mixed or obscured, affecting the accuracy of the results (Chen et al., 2018). Second, vegetation phenology is affected by many factors not considered here, such as the water cycle, insolation, altitude, and temperature (Du et al., 2019; Jochner et al., 2012; Shen et al., 2011). Future studies should use high-resolution remote sensing data to further assess changes in vegetation phenology along URGs with respect to the comprehensive impact that multiple factors have on vegetation phenology.

5. Conclusions

We used MOD13Q1, MCD12Q2, and MOD11A2 data for 2001–2017 to analyze the differences in vegetation phenology and land surface temperature along the URG in coastal Dalian sub-province, China. The results show that the marine monsoon climate caused coastal cities to have lower surface temperature and more precipitation than inland cities, resulting in vegetation phenology variations along the URG in coastal cities to be significantly smaller than for inland cities; △SOS was 7.4 d earlier and △EOS was 5.0 d later. These patterns reflect factors such as city size and ecological context (Walker et al., 2015; Wang et al., 2019a,b,c,d).

Our results provide a reference for studying long-term spatio-temporal change trends in vegetation phenology and LST along the URG in coastal cities. We show that it is possible to quantify the impact of coastal urbanization on the ecological environment, and to provide a strong basis for better understanding the agricultural development of coastal cities, but some uncertainties remain that need to be explored in future research.

CRediT authorship contribution statement

Jun Yang: Conceptualization, Methodology, Software. **Xue Luo:** Data curation, Software, Writing - review & editing. **Cui Jin:** Writing - review & editing. **Xiangming Xiao:** Writing - review & editing. **Jianhong Xia:** Writing - review & editing.

Declaration of Competing Interest

This manuscript has not been published or presented elsewhere in part or in entirety and is not under consideration by another journal. We have read and understood your journal's policies, and we believe that neither the manuscript nor the study violates any of these. There are no conflicts of interest to declare.

References

Balica, S.F., Wright, N.G., Van der Meulen, F., 2012. A flood vulnerability index for coastal cities and its use in assessing climate change impacts. Nat. Hazards 64, 73–105.
Bounoua, L., Zhang, P., Mostovoy, G., et al., 2015. Impact of urbanization on US surface climate. Environ. Res. Lett. 10, 1–9.
Busetto, L., Colombo, R., MigliavaccaI, M., et al., 2010. Remote sensing of larch phenological cycle and analysis of relationships with climate in the Alpine region. Glob. Change Biol. 16, 2504–2517.
Cao, R., Chen, Y., Shen, M., et al., 2018. A simple method to improve the quality of NDVI time-series data by integrating spatiotemporal information with the Savitzky-Golay filter. Remote Sens. Environ. 217, 244–257.
Chen, X., Xu, L., 2012. Temperature controls on the spatial pattern of tree phenology in China's temperate zone. Agric. For. Meteorol. 154-155, 195–202.
Chen, J., Jönsson, P., Tamura, M., et al., 2004. A simple method for reconstructing a high-quality NDVI time-series data set based on the Savitzky–Golay filter. Remote Sens. Environ. 91, 332–344.
Chen, M., Melaas, E.K., Gray, J.M., et al., 2016. A new seasonal-deciduous spring phenology submodel in the Community Land Model 4.5: impacts on carbon and water cycling under future climate scenarios. Glob. Change Biol. 22, 3675–3688.
Chen, X., Wang, D., Chen, J., et al., 2018. The mixed pixel effect in land surface phenology: a simulation study. Remote Sens. Environ. 211, 338–344.
Chen, Y., Sun, K., Chen, C., et al., 2019. Generation and evaluation of LAI and FPAR products from himawari-8 advanced himawari imager (AHI) data. Remote Sens-Basel 11, 1517.
Cong, N., Piao, S., Chen, A., et al., 2012. Spring vegetation green-up date in China inferred from SPOT NDVI data: a multiple model analysis. Agric. For. Meteorol. 165, 104–113.
Cui, Y., 2013. Preliminary estimation of the realistic optimum temperature for vegetation growth in China. Environ. Manage. 52, 151–162.
Deng, G., Zhang, H., Guo, X., et al., 2019. Asymmetric effects of daytime and nighttime warming on boreal forest spring phenology. Remote Sens. -Basel 11, 1651.
Du, J., He, Z., Piatek, K.B., et al., 2019. Interacting effects of temperature and precipitation on climatic sensitivity of spring vegetation green-up in arid mountains of China. Agric. For. Meteorol. 269-270, 71–77.
Forkel, M., Migliavacca, M., Thonicke, K., et al., 2015. Codominant water control on global interannual variability and trends in land surface phenology and greenness. Glob. Change Biol. 21, 3414–3435.
Fu, P., Weng, Q., 2018. Variability in annual temperature cycle in the urban areas of the United States as revealed by MODIS imagery. ISPRS J. Photogramm. 146, 65–73.
Fu, Y., He, H., Zhao, J., et al., 2018. Climate and spring phenology effects on autumn phenology in the Greater Khingan Mountains, Northeastern China. Remote Sens-Basel. 10, 449.
Garrity, S.R., Bohrer, G., Maurer, K.D., et al., 2011. A comparison of multiple phenology data sources for estimating seasonal transitions in deciduous forest carbon exchange. Agric. For. Meteorol. 151, 1741–1752.
Gazal, R., White, M.A., Gillies, R., et al., 2008. Globe students, teachers, and scientists demonstrate variable differences between urban and rural leaf phenology. Glob. Change Biol. 14, 1568–1580.
Geerken, R.A., 2009. An algorithm to classify and monitor seasonal variations in vegetation phenologies and their inter-annual change. ISPRS J. Photogramm. 64, 422–431.
Gill, A.L., Gallinat, A.S., Sanders-DeMott, R., et al., 2015. Changes in autumn senescence in northern hemisphere deciduous trees: a meta-analysis of autumn phenology studies. Ann. Bot. Lond. 116, 875–888.
Guo, A., Yang, J., Xiao, X., et al., 2020. Influences of urban spatial form on urban heat island effects at the community level in China. Sustain. Cities Soc. 53, 101972.
Han, G., Xu, J., 2013. Land surface phenology and land surface temperature changes along an urban–rural gradient in Yangtze River Delta, China. Environ. Manage. 52, 234–249.
Hanes, J.M., Schwartz, M.D., 2011. Modeling land surface phenology in a mixed temperate forest using MODIS measurements of leaf area index and land surface temperature. Theor. Appl. Climatol. 105, 37–50.
He, B., Ding, L., Prasad, D., 2019. Enhancing urban ventilation performance through the development of precinct ventilation zones: a case study based on the Greater Sydney, Australia. Sustain. Cities Soc. 47, 101472.
Hou, X., Gao, S., Niu, Z., et al., 2014. Extracting grassland vegetation phenology in North China based on cumulative SPOT-VEGETATION NDVI data. Int. J. Remote Sens. 35, 3316–3330.
Hu, K., Guo, Y., Yang, X., et al., 2019. Temperature variability and mortality in rural and urban areas in Zhejiang province, China: an application of a spatiotemporal index. Sci. Total Environ. 647, 1044–1051.
Jeganathan, C., Dash, J., Atkinson, P.M., 2014. Remotely sensed trends in the phenology of northern high latitude terrestrial vegetation, controlling for land cover change and vegetation type. Remote Sens. Environ. 143, 154–170.
Jeong, S., Schimel, D., Frankenberg, C., et al., 2017. Application of satellite solar-induced chlorophyll fluorescence to understanding large-scale variations in vegetation phenology and function over northern high latitude forests. Remote Sens. Environ. 190, 178–187.
Jochner, S.C., Sparks, T.H., Estrella, N., et al., 2012. The influence of altitude and urbanisation on trends and mean dates in phenology (1980–2009). Int. J. Biometeorol. 56, 387–394.
Jönsson, P., Eklundh, L., 2004. TIMESAT—a program for analyzing time-series of satellite sensor data. Comput. Geosci. U.K. 30, 833–845.
Krehbiel, C.P., Jackson, T., Henebry, G.M., 2016. Web-enabled Landsat data time series for monitoring urban heat island Impacts on land surface phenology. IEEE J.-Stars 9, 2043–2050.
Li, Z., Yang, P., Tang, H., et al., 2014. Response of maize phenology to climate warming in Northeast China between 1990 and 2012. Reg. Environ. Change 14, 39–48.
Li, X., Zhou, Y., Asrar, G.R., et al., 2016. Response of vegetation phenology to urbanization in the conterminous United States. Glob. Change Biol. Bioenergy 23, 2818–2830.
Liang, S., Shi, P., Li, H., 2016. Urban spring phenology in the middle temperate zone of China: dynamics and influence factors. Int. J. Biometeorol. 60, 531–544.
Liu, Q., Fu, Y.H., Zeng, Z., et al., 2016. Temperature, precipitation, and insolation effects on autumn vegetation phenology in temperate China. Glob. Change Biol. 22, 644–655.
Liu, Q., Fu, Y.H., Liu, Y., et al., 2017. Simulating the onset of spring vegetation growth across the Northern Hemisphere. Glob. Change Biol. 24, 1342–1356.
Liu, X., Yue, W., Yang, X., et al., 2020. Mapping urban heat vulnerability of extreme heat in hangzhou via comparing two approaches. Complexity 2020, 1–16.
Luo, Z., Sun, O.J., Ge, Q., et al., 2007. Phenological responses of plants to climate change in an urban environment. Ecol. Res. 22, 507–514.
Mariani, L., Parisi, S.G., Cola, G., et al., 2016. Climatological analysis of the mitigating effect of vegetation on the urban heat island of Milan, Italy. Sci. Total Environ. 569-570, 762–773.
NASA LP DAAC, 2015a. MOD13Q1: MODIS/Terra Vegetation Indices 16-Day l3 Global 250m SIN Grid v006. NASA EOSDIS Land Processes DAAC.
NASA LP DAAC, 2015b. MOD11A2: MODIS/Terra Land Surface Temperature and the Emissivity 8-Day l3 Global 1km SIN Grid v006. NASA EOSDIS Land Processes DAAC.
NASA LP DAAC, 2019. MCD12Q2: MODIS/Terra + Aqua Land Cover Type Yearly l3 Global 500m SIN Grid v006. NASA EOSDIS Land Processes DAAC.
Peng, S., Piao, S., Ciais, P., et al., 2012. Surface urban heat island across 419 global big cities. Environ. Sci. Technol. 46, 696–703.
Ren, Q., He, C., Huang, Q., et al., 2018. Urbanization impacts on vegetation phenology in China. Remote Sens. -Basel 10, 1905.
Richardson, A.D., Keenan, T.F., Migliavacca, M., et al., 2013. Climate change, phenology, and phenological control of vegetation feedbacks to the climate system. Agric. For. Meteorol. 169, 156–173.
Sakamoto, T., 2018. Refined shape model fitting methods for detecting various types of phenological information on major U.S. crops. ISPRS J. Photogramm. 138, 176–192.
Schaber, J., Badeck, F., 2005. Plant phenology in Germany over the 20th century. Reg. Environ. Change 5, 37–46.
Senf, C., Pflugmacher, D., Heurich, M., et al., 2017. A Bayesian hierarchical model for estimating spatial and temporal variation in vegetation phenology from Landsat time series. Remote Sens. Environ. 194, 155–160.
Shen, M., Tang, Y., Chen, J., et al., 2011. Influences of temperature and precipitation before the growing season on spring phenology in grasslands of the central and eastern Qinghai-Tibetan Plateau. Agric. For. Meteorol. 151, 1711–1722.
Sohoulande Djebou, D.C., Singh, V.P., Frauenfeld, O.W., 2015. Vegetation response to precipitation across the aridity gradient of the southwestern United states. J. Arid Environ. 115, 35–43.
Stewart, I.D., Oke, T.R., 2012. Local climate zones for urban temperature studies. B Am. Meteorol. Soc. 93, 1879–1900.
Tan, B., Morisette, J.T., Wolfe, R.E., et al., 2011. An enhanced TIMESAT algorithm for estimating vegetation phenology metrics from MODIS data. IEEE J. Stars 4, 361–371.
Tarawally, M., Xu, W., Hou, W., et al., 2018. Comparative analysis of responses of Land Surface Temperature to long-term land use/cover changes between a coastal and inland city: a case of freetown and Bo Town in Sierra Leone. Remote Sens. Basel 10, 112.
van der Tol, C., Rossini, M., Cogliati, S., et al., 2016. A model and measurement comparison of diurnal cycles of sun-induced chlorophyll fluorescence of crops. Remote Sens. Environ. 186, 663–677.
Verger, A., Filella, I., Baret, F., et al., 2016. Vegetation baseline phenology from kilometric global LAI satellite products. Remote Sens. Environ. 178, 1–14.
Villa, P., Pinardi, M., Bolpagni, R., et al., 2018. Assessing macrophyte seasonal dynamics using dense time series of medium resolution satellite data. Remote Sens. Environ. 216, 230–244.
Vintrou, E., Bégué, A., Baron, C., et al., 2014. A comparative study on satellite- and model-based crop phenology in West Africa. Remote Sens-Basel 6, 1367–1389.
Walker, J.J., de Beurs, K.M., Henebry, G.M., 2015. Land surface phenology along urban to rural gradients in the U.S. Great Plains. Remote Sens. Environ. 165, 42–52.
Walther, S., Voigt, M., Thum, T., et al., 2016. Satellite chlorophyll fluorescence measurements reveal large-scale decoupling of photosynthesis and greenness dynamics in boreal evergreen forests. Glob. Change Biol. 22, 2979–2996.
Wang, C., Cao, R., Chen, J., et al., 2015. Temperature sensitivity of spring vegetation phenology correlates to within-spring warming speed over the Northern Hemisphere. Ecol. Indic. 50, 62–68.
Wang, X., Gao, Q., Wang, C., et al., 2017. Spatiotemporal patterns of vegetation phenology change and relationships with climate in the two transects of East China. Glob. Ecol. Conserv. 10, 206–219.
Wang, G., Huang, Y., Wei, Y., et al., 2019a. Inner Mongolian grassland plant phenological changes and their climatic drivers. Sci. Total Environ. 683, 1–8.
Wang, S., Ju, W., Penuelas, J., et al., 2019b. Urban-rural gradients reveal joint control of elevated CO2 and temperature on extended photosynthetic seasons. Nat. Ecol. Evol. 3, 1076–1085.
Wang, Y., Li, Y., Qiao, Z., et al., 2019c. Inter-city air pollutant transport in the Beijing-Tianjin-Hebei urban agglomeration: comparison between the winters of 2012 and 2016. J. Environ. Manage. 250, 109520.
Wang, Y., Luo, Y., Shafeeque, M., 2019d. Interpretation of vegetation phenology changes

using daytime and night-time temperatures across the Yellow River Basin, China. Sci. Total Environ. 693, 1–12.
Weng, Q., Lu, D., Schubring, J., 2004. Estimation of land surface temperature–vegetation abundance relationship for urban heat island studies. Remote Sens. Environ. 89, 467–483.
White, M.A., Beurs, D., Kirsten, M., et al., 2009. Intercomparison, interpretation, and assessment of spring phenology in North America estimated from remote sensing for 1982–2006. Glob. Change Biol. 15, 2335–2359.
Workie, T.G., Debella, H.J., 2018. Climate change and its effects on vegetation phenology across ecoregions of Ethiopia. Glob. Ecol. Conserv. 13, 1–13.
Wu, C., Hou, X., Peng, D., et al., 2016. Land surface phenology of China's temperate ecosystems over 1999–2013: spatial–temporal patterns, interaction effects, covariation with climate and implications for productivity. Agric. For. Meteorol. 216, 177–187.
Xie, P., Yang, J., Wang, H., et al., 2020. A New method of simulating urban ventilation corridors using circuit theory. Sustain. Cities Soc. 59, 102162.
Xin, Q., Broich, M., Zhu, P., et al., 2015. Modeling grassland spring onset across the Western United States using climate variables and MODIS-derived phenology metrics. Remote Sens. Environ. 161, 63–77.
Yang, J., Sun, J., Ge, Q., et al., 2017. Assessing the tmpacts of urbanization-associated green space on urban land surface temperature: a case study of Dalian, China. Urban For. Urban Green. 22, 1–10.
Yang, J., Wang, Y., Xiao, X., et al., 2019. Spatial differentiation of urban wind and thermal environment in different grid sizes. Urban Clim. 28, 100458.
Yao, R., Wang, L., Huang, X., et al., 2017. Investigation of urbanization effects on Land surface phenology in Northeast China during 2001–2015. Remote Sens-Basel 9, 66.
Yu, H., Luedeling, E., Xu, J., 2010. Winter and spring warming result in delayed spring phenology on the Tibetan Plateau. Proc. Natl. Acad. Sci. U. S. A. 107, 22151–22156.
Yu, X., Wang, Q., Yan, H., et al., 2014. Forest phenology dynamics and its Responses to meteorological variations in Northeast China. Adv. Meteorol. 2014, 1–12.
Yu, L., Liu, T., Bu, K., et al., 2017. Monitoring the long term vegetation phenology change in Northeast China from 1982 to 2015. Sci. Rep. U. K. 7, 1–9.
Yuan, H., Wu, C., Lu, L., et al., 2018. A new algorithm predicting the end of growth at five evergreen conifer forests based on nighttime temperature and the enhanced vegetation index. ISPRS J. Photogramm. 144, 390–399.
Zhang, X., Friedl, M.A., Schaaf, C.B., et al., 2004. The footprint of urban climates on vegetation phenology. Geophys. Res. Lett. 31 n/a-n/a.
Zhang, X., Friedl, M.A., Schaaf, C.B., 2006. Global vegetation phenology from Moderate Resolution Imaging Spectroradiometer (MODIS): evaluation of global patterns and comparison with in situ measurements. J. Geophys. Res. Biogeosci. 111, 1–14.
Zhang, Q., Kong, D., Shi, P., et al., 2018. Vegetation phenology on the Qinghai-Tibetan Plateau and its response to climate change (1982–2013). Agric. For. Meteorol. 248, 408–417.
Zhao, J., Zhang, H., Zhang, Z., et al., 2015. Spatial and temporal changes in vegetation phenology at middle and high latitudes of the Northern Hemisphere over the past three decades. Remote Sens. -Basel 7, 10973–10995.
Zhao, J., Wang, Y., Zhang, Z., et al., 2016. The variations of land surface phenology in Northeast China and its responses to climate change from 1982 to 2013. Remote Sens. -Basel 8, 400.
Zheng, J., Zhong, S., Ge, Q., et al., 2013. Changes of spring phenodates for the past 150 years over the Yangtze River Delta. J. Geogr. Sci. 23, 31–44.
Zhong, Q., Ma, J., Zhao, B., et al., 2019. Assessing spatial-temporal dynamics of urban expansion, vegetation greenness and photosynthesis in megacity Shanghai, China during 2000–2016. Remote Sens. Environ. 233, 1–12.
Zhou, D., Zhao, S., Zhang, L., et al., 2016. Remotely sensed assessment of urbanization effects on vegetation phenology in China's 32 major cities. Remote Sens. Environ. 176, 272–281.
Zikra, M., Suntoyo, Lukijanto, 2015. Climate change impacts on Indonesian coastal areas. Procedia Earth Planet. Sci. 14, 57–63.
Zipper, S.C., Schatz, J., Singh, A., et al., 2016. Urban heat island impacts on plant phenology: intra-urban variability and response to land cover. Environ. Res. Lett. 11, 1–12.